SCIENCE CHINA
Technological Sciences

•Article•

February 2021 Vol.64 No.2: 423–432
https://doi.org/10.1007/s11431-020-1674-7

Robust, healable and hydrophobically recoverable polydimethylsiloxane based supramolecular material with dual-activate hard segment

LV Chi[1], QI YuHao[1], HU RuoFei[2*] & ZHENG JunPing[1*]

[1] *Tianjin Key Laboratory of Composite and Functional Materials, School of Materials Science and Engineering, Tianjin University, Tianjin 300350, China;*
[2] *College of Chemistry and Chemical Engineering, Dezhou University, Dezhou 253023, China*

Received April 25, 2020; accepted June 11, 2020; published online November 18, 2020

In this paper, a novel dual-activate hard segment strategy is proposed for the fabrication of polydimethylsiloxane (PDMS) based supramolecular polymer (PDMS-PDITC-IPDI). The unique design endows the PDMS-PDITC-IPDI with high toughness (43.1–24.5 MJ/m^3), tensile strength (11.3–6.6 MPa) and elongation at break (730%–615%), and the mechanical properties and dynamic property can be regulated by varying degrees of hard segment activation. Moreover, the PDMS-PDITC-IPDI polymers exhibit excellent self-recovery property during successive loading-unloading processes. Additionally, both wettability damage caused by O_2 plasma treatment and mechanical damage can be healed by simple heating, showing good hydrophobic recovery and self-healability. Taking advantages of merits of the PDMS-PDITC-IPDI, the applications of the material as recyclable adhesive and 3D printing material are also investigated.

high strength, hydrophobic recovery, self-healing, PDMS, 3D printing

Citation: Lv C, Qi Y H, Hu R F, et al. Robust, healable and hydrophobically recoverable polydimethylsiloxane based supramolecular material with dual-activate hard segment. Sci China Tech Sci, 2021, 64: 423–432, https://doi.org/10.1007/s11431-020-1674-7

1 Introduction

Benefitting from the unique molecular structure, polydimethylsiloxane (PDMS) based materials exhibit fascinating hydrophobicity, flexibility and nontoxicity [1–3]. In recent years, they are widely used in adhesives, sealants and coatings, etc. [4–6]. High mechanical strength and toughness are first required for these applications. Unfortunately, most neat PDMS based materials usually show poor mechanical properties, which makes them more likely to damage in their service life and limits their practical applications. To address this problem, people have tried to design PDMS materials capable of healing themselves or recycling their wastes [7–11]. Nevertheless, self-healing materials often involve in weak dynamic bonds and their mechanical properties are often compromised. Mechanically strong and tough self-healing materials are urgently desired but the preparation still a challenge.

Regarding to robust and tough self-healing materials, many design strategies have been proposed and demonstrated. The most common approach is to introduce nanoparticles. However, the introduction of nanoparticles involves complicated process of modification and dispersion and has been confirmed to reduce polymer chain mobility, thus decreasing the self-healability [12,13]. Another alternative method is to construct double-network systems. Nevertheless, they often exhibit low self-healing efficiency due to the presence of the permanent crosslinked network [14–16]. Taking the balance of contradiction between mechanical properties and dynamic property into account, su-

*Corresponding authors (email: huruofei@tju.edu.cn; jpzheng@tju.edu.cn)

pramolecular hydrogen bonding strategy is promising and frequently used. As typical supramolecular interaction, hydrogen bond has attracted more and more attention because of its flexible operability and tunable bond strength [17–20]. Theoretically, supramolecular self-healing materials could realize infinite healing times, so they are more competitive in practical applications [21]. Previous studies have shown that introducing hydrogen bond units has a significant effect on the mechanical properties due to the crystallization of hydrogen bond and micro-phase separation [22]. However, excessive crystallization of hydrogen bond often results in poor dynamic property, which is detrimental to self-healing performance. In order to avoid the adverse effect of crystallization, weak hydrogen bond unit and low hydrogen bond density are usually adopted, but those results in a substantial decrease in tensile strength [9,23]. Robust and tough self-healing PDMS materials are still rarely reported. Xu et al. [23] prepared a PDMS material via multiphase active method. The tensile strength is less than 0.1 MPa. Wu et al. [24] designed a supramolecular PDMS material by sacrificial hydrogen bonds. The tensile strength is 2.6 MPa. Zhang et al. [25] prepared a self-healing polysiloxane material via hierarchical crosslinked networks. Although the tensile strength is up to 8.6 MPa, the elongation at break is only 224%.

In addition to mechanical properties, multi-functionality is also desired. Hydrophobic materials have potential applications in antifouling, self-cleaning and oil/water separation fields [26,27], wettability recovery after chemical damage can greatly expand their application value. However, a majority of reported self-healing materials can only repair mechanical damage, the surface wettability cannot be recovered after chemical damage. Self-healing materials with wettability recovery are still rarely reported [28,29]. 3D printing is a novelty additive manufacturing technique to rapidly create complex structures and geometries. Temperature and UV-induced crosslinking are the overwhelming 3D printing methods for silicone elastomers. These two methods inevitably involve curing agent, high temperature and many other factors, which increase the complexity of 3D printing. Especially for strong supramolecular polymers, high temperature is more unavoidable due to the strong interaction. Hence, it is imperative to design room-temperature 3D printing silicone materials via a more facile approach.

Rational hard segment design can take into account the above performances. In this work, we put forward a "dual-activate hard segment strategy" by introducing aromatic ring thiourea and urea units as hard segments. Due to the amorphous structure, thiourea units could break the crystalline structure of the urea units and thus effectively prevents crystallization. Meanwhile, urea units could disturb the strong π-π stacking interactions between aromatic rings and thus prevents excessive interaction. This dual-activate effect can endow the material with appropriate dynamic property while sufficient to ensure mechanical strength. Different from the previously reported improvement of self-healability by introducing weak interactions or reducing hydrogen bond density, in this strategy, we get the improved self-healability via the mutual activation of two strong interaction units, which avoids the sharp decline in mechanical strength that might result from direct introduction of weak interactions. This effectively reconciles the dynamic property and the mechanical performance of the material. The obtained PDMS materials exhibit different degrees of hard segment activation by changing chemical composition, thus showing tunable high mechanical properties. In addition, the PDMS materials possess excellent self-recovery property. Upon mechanical or surface chemical damage, they show high-efficient repair of mechanical properties and surface hydrophobicity. Furthermore, due to the dual-activate design in the hard segment, the prepared PDMS materials are also endowed with additional high adhesive property and 3D printing processability.

2 Experimental

Materials Bis (3-aminopropyl)-terminated poly(dimethylsiloxane) (H_2N-PDMS-NH_2, M_n = 1000 g mol^{-1}) was purchased from Heowns. Isophorone diisocyanate (IPDI) was obtained from Rhawn Chemicals. *p*-phenylene diisothlocyanate (PDITC) was purchased from Nine Ding Chemicals. Anhydrous tetrahydrofuran (THF) and dimethylformamide were supplied by Heowns. H_2N-PDMS-NH_2 was dried under reduced pressure for 2 h at 100°C prior to use. All other reagents were chemically grade and used without further purification.

Preparation of PDMS-PDITC-IPDI and control samples PDMS-PDITC-IPDI was synthesized via a facile one-pot procedure. First, H_2N-PDMS-NH_2 was added in a three-neck bottle and dissolved in THF. Then, a stoichiometric amount IPDI and PDITC were dissolved in THF/DMF mixed solvent. Subsequently, the mixture solution was added dropwise into the above H_2N-PDMS-NH_2 solution. The reaction was conducted under nitrogen at 30°C. After being stirred 2 d, the reaction solution was poured into a fluoridated mold for dry and the polymer obtained (molar ratios of reactants: PDMS-$PDITC_{0.1}$-$IPDI_{0.9}$, H_2N-PDMS-NH_2/PDITC/IPDI=1∶0.1∶0.9; PDMS-$PDITC_{0.2}$-$IPDI_{0.8}$, H_2N-PDMS-NH_2/PDITC/IPDI=1∶0.2∶0.8; PDMS-$PDITC_{0.3}$-$IPDI_{0.7}$, H_2N-PDMS-NH_2/PDITC/IPDI=1∶0.3∶0.7; PDMS-$PDITC_{0.4}$-$IPDI_{0.6}$, H_2N-PDMS-NH_2/PDITC/IPDI=1∶0.4∶0.6). Control samples PDMS-IPDI and PDMS-PDITC were synthesized by a similar method (molar ratios of reactants: PDMS-IPDI, H_2N-PDMS-NH_2/IPDI=1∶1; PDMS-PDITC, H_2N-PDMS-NH_2/PDITC=1∶1). Due to the poor re-solubility, PDMS-PDITC test sample was obtained by hot-press at 120°C.

Characterizations ^{1}H-nuclear magnetic resonance (^{1}H NMR) spectrum was recorded on a AVANCE IIITM HD 400 MHz spectrometer (Bruker, China) at room temperature. Gel permeation chromatography (GPC) measurements were carried out by a Waters (USA) instrument equipped with 515 HPLC pump, eluted with THF at 1 mL/min and polystyrene standards as reference. Fourier-transform infrared (FT-IR) spectra were recorded on a Nicolet (USA) 6700 spectrometer (attenuated total reflectance method) from 4000 to 650 cm^{-1}. Thermal gravimetric analysis (TGA) was carried out on a Netzsch (Germany) STA449F3 thermal analyser (heating temperature range: 40°C–700°C, heating rate: 10°C min^{-1}, atmosphere: Ar). UV-vis transmittance spectra were recorded by an Agilent spectrophotometer with linearity calibratn filter kit Cary 500. Differential scanning calorimetry (DSC) tests were carried out on a Waters (USA) Q2000 (temperature range: −90°C to 150°C, heating rate: 10°C min^{-1}, atmosphere: N_2). X-ray diffraction (XRD) tests were conducted on a Bruker (Germany) D8 advanced diffractometer, and the 2θ were recorded from 10° to 70°. Dynamic mechanical analysis (DMA) was measured using TA (USA) Q800 instrument with a strain of 0.1% and a frequency of 1 Hz, heating rate: 10°C min^{-1}.

Mechanical tests Stress relaxation measurements were performed with a SANS CMT4203 universal testing machine (China). The samples were applied to 100% strain and relaxation time of the stress was 1000 s. The stress-strain curves and loading-unloading cycles were obtained by using a SANS CMT4203 universal testing machine with stretching rate of 10 mm/min. The adhesion strength was obtained by shear tensile test using a SANS CMT4203 universal testing machine with stretching rate of 10 mm/min. The toughness was characterized by fracture energy, which is defined as the area below the stress-strain curve. The recovery ratio was defined by a ratio of energy dissipation after different resting time to the initial cycle. The dissipated energy is defined as the area of the hysteresis loop encompassed by the loading-unloading curve.

Mechanical self-healing tests The polymer samples were cut and then the damaged samples were placed in a polytetrafluoroethylene dish for healing at 100°C. After standing for several hours, the self-healed samples were tested. Self-healing efficiency was characterized through the toughness. Scanning electron microscope (SEM) images of the scratch were obtained using a Hitachi (Japan) SU1510 tungsten filament scanning electron microscope.

Chemical self-healing tests O_2 plasma etching was conducted by YZD08-5C plasma cleaner (China). The power of the cleaner was 50 W. The static water contact angles (SWCA) before and after chemical damage was measured by using a JC 2000D Water contact angle meter (China).

3D printing process The 3D printing process was carried out via a modified core *XY*-double *Z* axis motion platform with mechanical extrusion device. The high concentration solution for 3D printing was prepared by dissolving the PDMS-PDITC-IPDI (1.5 g) in THF (0.5 mL).

3 Results and discussion

3.1 Material design and characterization

In this work, PDITC and IPDI were chosen to fabricate PDMS based supramolecular material based on the novel dual-activate hard segment strategy. As shown in Figure 1(a),

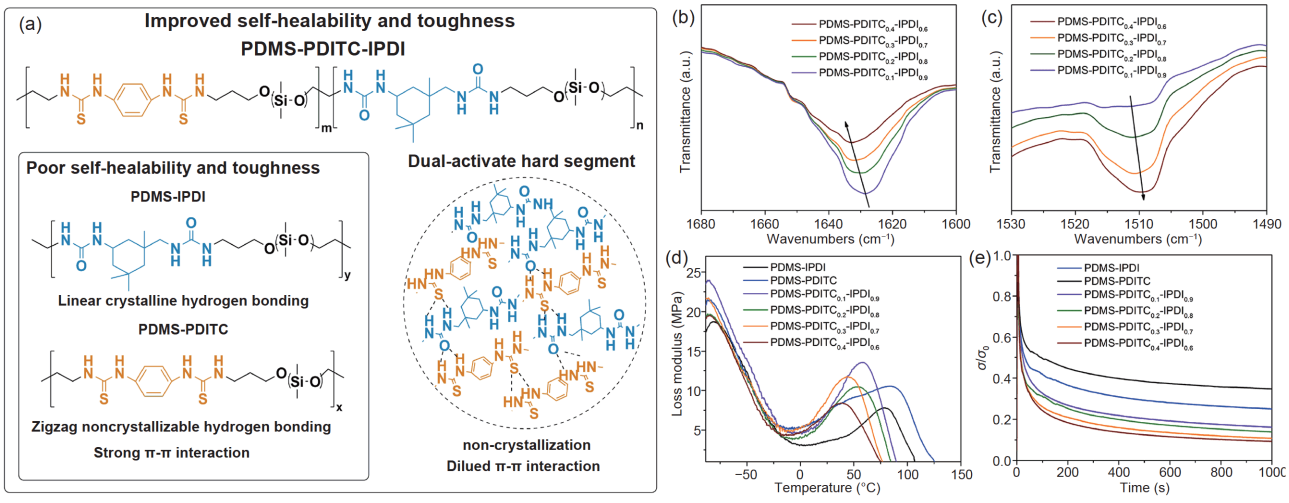

Figure 1 (Color online) (a) Design concept and chemical structure of the PDMS-PDITC-IPDI supramolecular material; (b) comparison of FT-IR absorption peaks of carbonyl group (C=O) in PDMS-PDITC-IPDI materials with different chemical composition; (c) comparison of FT-IR absorption peaks of thiocarbonyl group (C=S) in PDMS-PDITC-IPDI materials with different chemical composition; (d) the loss modulus-temperature curves of PDMS-IPDI, PDMS-PDITC and PDMS-PDITC-IPDI materials; (e) normalized room temperature stress relaxation curves of PDMS-IPDI, PDMS-PDITC and PDMS-PDITC-IPDI materials with a strain of 100%.

PDMS-PDITC-IPDI polymers were prepared with varied molar ratios of PDITC and IPDI. ^{1}H NMR, FT-IR and GPC data are provided in Figures S1, S2 and Table S1. The results confirmed that the PDMS-PDITC-IPDI polymers have been successfully synthesized. TGA test was also performed. The result showed that the PDMS-PDITC-IPDI has excellent thermal stability with initial decomposition temperature of 200°C (Figure S3).

To illustrate the concept of this strategy, two control samples PDMS-IPDI and PDMS-PDITC were prepared. PDMS-IPDI appears translucent due to the hard segment crystallization, which was verified by the DSC test (Figure S4). An obvious crystallization peak was observed on the DSC curve of PDMS-IPDI. In contrast, no crystallization peak was found on the DSC curve of PDMS-PDITC, suggesting the amorphous state of PDMS-PDITC. We attribute this phenomenon to the noncrystallizable zigzag thiourea hydrogen bonds [30]. Further, XRD tests were performed to demonstrate the amorphous or crystalline state of PDMS-PDITC and PDMS-IPDI (Figure S5). Note that both PDMS-IPDI and PDMS-PDITC show poor self-healability (Figure S6). This could be attributed to the strong π-π stacking interaction and crystallization-restricted chain mobility, which greatly limits the activity of PDITC-PDITC linkages and IPDI-IPDI linkages within hard segment. In this strategy, PDITC and IPDI are implanted simultaneously. The PDITC motifs could break the crystalline structure of IPDI motifs and in turn IPDI motifs could prevent excessive π-π stacking interactions. This synergistic effect results in increased hard segment activity. DSC tests were conducted to investigate the transition of PDMS-PDITC-IPDI from crystallization to amorphous. As shown in Figure S7, crystallization peak was not detected, indicating amorphous state of PDMS-PDITC-IPDI. Besides, PDMS-PDITC-IPDI is transparent. A PDMS-PDITC-IPDI film coating on glass slide exhibited an average transmittance of more than 90% under visible light wavelengths (400–800 nm) (Figure S8).

FT-IR was applied to investigate the changes of hydrogen bonding. As shown in Figure 1(b) and (c), there are two characteristic peaks at about 1628 and 1512 cm^{-1} for PDMS-PDITC$_{0.1}$-IPDI$_{0.9}$. They are assigned to the stretching vibration of carbonyl group (C=O) and thiocarbonyl group (C=S), respectively. Obviously, with the increase of PDITC ratio, the C=O peak shifted to a higher wavenumber with decreasing peak strength, while C=S peak shifted to a lower wavenumber with increasing peak strength. It is well known that higher wavenumber represents lower hydrogen bond strength, indicating that hydrogen bonds begin to change from order to disorder. The changes in peak position imply change in hydrogen bond activity. At low PDITC ratio, the carbonyl groups are dominant. So carbonyl groups are more likely to form ordered urea-urea hydrogen bonds, which lead to the lower wavenumber and higher peak strength. On the contrary, abundant carbonyl groups make it difficult to form ordered thiourea-thiourea hydrogen bonds, resulting in a higher wavenumber and lower peak strength of thiocarbonyl group. With the increase of PDITC ratio, the number of thiocarbonyl group increased. The thiourea-thiourea hydrogen bonds are more likely to form in order. Meanwhile, the urea-urea hydrogen bonds begin to change from order to disorder.

In addition, hierarchical interactions may exist. The density functional theory (DFT) simulated calculation further verified that hydrogen bonds in hard segment exhibited different interaction energies (Figure S9). As a comprehensive result, PDMS-PDITC-IPDI materials exhibit the activated hard segment. DMA test were performed to verify this. As seen in Figure 1(d), intense peaks appear in the loss modulus-temperature curves. The temperature corresponding to the peak can be considered as the glass transition temperature (T_g) of the hard segment under dynamic viscoelastic conditions. Comparatively, PDMS-PDITC-IPDI materials show lower T_g of hard segment compared with PDMS-IPDI and PDMS-PDITC. And the T_g decreases with the increase of PDITC ratio for PDMS-PDITC-IPDI, indicating different levels of activation of hard segment. Stress relaxation experiments were also carried out. As shown in Figure 1(e). The results showed that the rate of stress relaxation of PDMS-PDITC-IPDI materials is faster than that of PDMS-PDITC and PDMS-IPDI, implying the improved hard segment activity. Notably, the rate of stress relaxation increases with the increase of PDITC ratio, which is consistent with the results of DMA tests. In conclusion, the above results showed that the dual-activate hard segment strategy is effective. The materials with different degree of activation can be obtained by changing the ratio of PDITC, which implies the tunable mechanical properties.

3.2 Mechanical properties of PDMS-PDITC-IPDI materials

The stress-strain curves of PDMS-PDITC-IPDI materials were obtained by a universal tensile machine at a stretching rate of 10 mm/min. As seen in Figure 2(a), PDMS-PDITC-IPDI materials exhibit excellent mechanical properties. The mechanical properties data are provided in Table S2. In particular, the elastic modulus, tensile strength and elongation at break of PDMS-PDITC$_{0.2}$-IPDI$_{0.8}$ are as high as 20.2, 11.3 MPa and 703%, respectively. The overall mechanical performance is better than most self-healing polysiloxane materials reported previously [31–44] (Figure 2(b), Table S3). In terms of stretchability, the PDMS-PDITC-IPDI materials are significantly higher to the control samples PDMS-PDITC and PDMS-IPDI. The elongation at break of PDMS-PDITC and PDMS-IPDI are only 315% and 460% respectively (see Figure S4). The increased stretchability can be

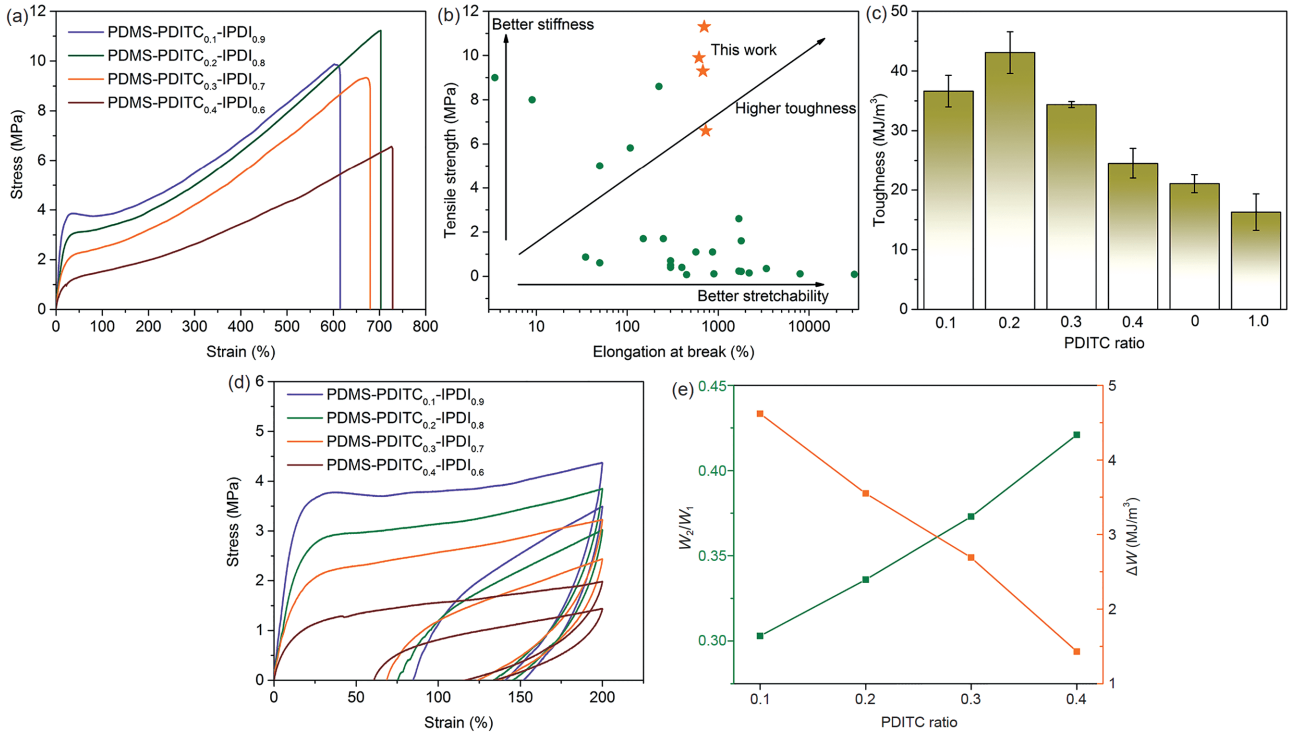

Figure 2 (Color online) (a) Stress-strain curves of PDMS-PDITC-IPDI materials with different chemical composition; (b) comparison of mechanical properties between our material and self-healing polysiloxane materials previously reported; (c) comparison of toughness of PDMS-IPDI, PDMS-PDITC and PDMS-PDITC-IPDI materials, the PDITC ratio of PDMS-IPDI and PDMS-PDITC are 0 and 1.0, respectively; (d) successive loading-unloading curves of PDMS-PDITC-IPDI materials; (e) dependence of W_2/W_1 and ΔW for PDMS-PDITC-IPDI materials at various PDITC ratios.

attributed to the weakened interactions caused by activated hard segments. As can be seen from the stress-strain curves, with the increase of PDITC ratio, PDMS-PDITC-IPDI materials showed a transition from plasticity to elasticity. For PDMS-PDITC$_{0.1}$-IPDI$_{0.9}$, an obvious yield process can be observed, indicating the plastic deformation. When the ratio of PDITC increases to 0.4, PDMS-PDITC$_{0.4}$-IPDI$_{0.6}$ exhibited an elastic behavior. The reason of this phenomenon can be attributed to the improvement of hard segment dynamic property. When the content of PDITC is low, the stronger hard segment interaction makes the material's deformation recovery ability become worse, leading to plastic deformation. As the content of PDITC increases, the interaction becomes less strong, which increases the ability of the material to recover from deformation and thus exhibit elasticity. As a result of the equilibrium between elasticity and plasticity, the prepared PDMS-PDITC-IPDI materials exhibited high toughness. Figure 2(c) shows the comparison data of toughness between PDMS-PDITC-IPDI materials and PDMS-PDITC and PDMS-IPDI. In terms of PDMS-PDITC-IPDI materials, the toughness value increases first and then decreases with the increase of PDITC ratio. When the PDITC ratio is 0.2, the toughness reaches the maximum of 43.1 MJ/m^3. The toughness value is 2.1 times and 2.7 times that of the control samples PDMS-IPDI and PDMS-PDITC, respectively.

To further investigate the energy dissipation behavior, successive cyclic tensile tests for PDMS-PDITC-IPDI materials were conducted with a certain strain of 200%. The hysteresis loop during the loading-unloading process reflects the energy dissipation. As seen from Figure 2(d), all PDMS-PDITC-IPDI materials showed significant hysteresis during the first tensile cycle, indicating great energy dissipation capacity. The second tensile cycles followed, but showed less hysteresis. The energy dissipation capacity can be quantified by the hysteresis ratio between successive two cycles (W_2/W_1), where W_1 and W_2 represent the dissipating energy of the first and second loading-unloading cycle, respectively [45]. A higher hysteresis ratio represents lower energy dissipation. The comparison of hysteresis ratio is shown in Figure 2(e). With increasing PDITC ratio, the hysteresis ratio exhibits a monotonically increasing trend, indicating decreasing energy dissipation capacity. The difference of hysteresis ratio likely attributed to the different yield behavior. A more yielding material usually means a greater dissipation of energy, thus leading higher energy dissipation capacity.

Self-recovery ability is the important property of materials, particularly for those materials that involve back-and-forth loading and unloading in practical use. Since PDMS-PDITC-IPDI is physically crosslinked through hydrogen bonds, the dissociated hydrogen bonds can be recovered under certain conditions. Taking PDMS-PDITC$_{0.2}$-IPDI$_{0.8}$ as an example,

7-times successive loading-unloading cycles are performed. During the loading-unloading tests, the strain gradually increased from 50% to 600% and resting time is not allowed between any two successive tensile cycles. As seen in Figure 3(a), the material exhibited prominent hysteresis and strain softening behavior. The hysteresis loops became larger as the strain increases, and the maximum tensile strength of each cycle is lower than that of the corresponding value in the stress-strain curve. These results indicated the occurrence of the internal fracture of the network by deformation. Besides, the adjacent two hysteresis loops overlapped with each other but the hysteresis loops did not completely coincide, indicating that partial recovery can be achieved in the case of energy dissipation caused by stretching. After the first loading-unloading cycles, the material sample was placed at room temperature for 24 h and then retested. Based on the maximum tensile strength, 95% recovery was realized (Figure 3(b)). Similar 5-times successive loading-unloading cycles were carried out at small certain strain of 200%. After resting 12 h at room temperature, the second successive loading-unloading curves were almost completely recovered to the first successive loading-unloading curves (Figure 3(c) and (d)). To show the self-recovery performance more visually, the self-recovery process was recorded through digital photos. As shown in Figure S10, cyclic tensile test was carried on a material film of 14.0 mm in length. After the two loading-unloading cycles, the length of the material film increases to 19.0 mm. After resting for a period of time at room temperature, the length eventually returned to 14.8 mm after 5 h, indicating the good dimensional recovery. The self-recovery ability was further quantitatively evaluated. As shown in Figure 3(e), with the extension of the resting time, the hysteresis loop was gradually recovered to the first hysteresis loop. After resting for 4 h, the area of hysteresis loops was largely recovered with the recovery ratio of 94%. High temperature can accelerate the recovery process. As shown in Figure 3(f), the recovery ratio is up to 95% just after resting 30 min at 80°C. The above results demonstrate the excellent self-recovery ability of the PDMS-PDITC-IPDI material.

3.3 Self-healability and hydrophobic recovery of PDMS-PDITC-IPDI materials

The dual-activate hard segment strategy also endows the PDMS-PDITC-IPDI material with enhanced self-healability. For a more intuitive demonstration of self-healing performance, the scratch self-healability was evaluated by SEM firstly. As can be seen from Figure 4(a), the original material has a distinct scratch on its surface. After healed at 100°C for 60 min, the scratch disappeared completely, indicating the excellent self-healability. For further quantitative evaluation of self-healability, the PDMS-PDITC-IPDI material before and after self-healing was tested by mechanical tensile test. Figure 4(b) shows the stress-strain curves of the healed PDMS-PDITC$_{0.2}$-IPDI$_{0.8}$ material with different healing times. With the extension of healing time, both the elongation at break and tensile strength are gradually recovered. The self-healing efficiency was provided in Figure 4(c). As shown, a self-healing efficiency up to 90.7% was obtained after healing at 100°C for 8 h. Furthermore, the self-healability of PDMS-PDITC-IPDI materials with different PDITC ratio was investigated (Figure 4(d)). Uniformly, the self-healing time of all materials is 8 h. As the PDITC ratio increases, the self-healing efficiencies of PDMS-PDITC-IPDI materials are 77.5%, 90.2%, 94.7% and 95.2%, respectively. The difference of self-healing efficiencies can be contributed to the fact that different levels of activation of hard segment. However, for PDMS-IPDI and PDMS-PDITC, the self-healing efficiencies are only 57.7% and 25.7%, respectively (see Figure S6). It is worth mentioning that the prepared PDMS-PDITC-IPDI material was able to recover its wettability after chemical damage. As shown in Figure 4(e), the original PDMS-PDITC-IPDI material showing good hydrophobicity with a static water contact angle (SWCA) of 110°. To evaluate the chemical self-healability, the PDMS-PDITC-IPDI material was treated by O_2 plasma etching for 1 min. Due to the oxidation of O_2 plasma etching, the surface of etched material became hydrophilic with a SWCA of 12°. Nevertheless, the hydrophilic surface can completely recover its hydrophobicity after being heated at 100°C for 30 min. At room temperature, the PDMS-PDITC-IPDI material also showed a certain chemical self-healability. The SWCA recovered to 70° in 12 h (Figure S11). The hydrophobic recovery is attributed to the dynamic activated hard segment and the mobility of the soft segment. During the heat treatment, these polar groups were diffused into the material interior and the PDMS segments migrated to the surface via thermodynamically driven rearrangement, leading the recovery of hydrophobicity. The restorable wettability endows the material with great application potential in the field of hydrophobic coating.

3.4 Multifunctional applications of PDMS-PDITC-IPDI

Given the combination of so many excellent performances in mechanical and chemical aspects, the prepared PDMS-PDITC-IPDI material has the potential for use in various industrial applications. The comprehensive performance comparison is provided in Table S3. Besides, our materials are soluble in various organic solvents (Figure S12), while other supramolecular hydrogen bonding materials with such high strength are usually insoluble due to the strong interaction energy. The excellent solubility endows the PDMS-PDITC-IPDI material with desired recyclability and makes it

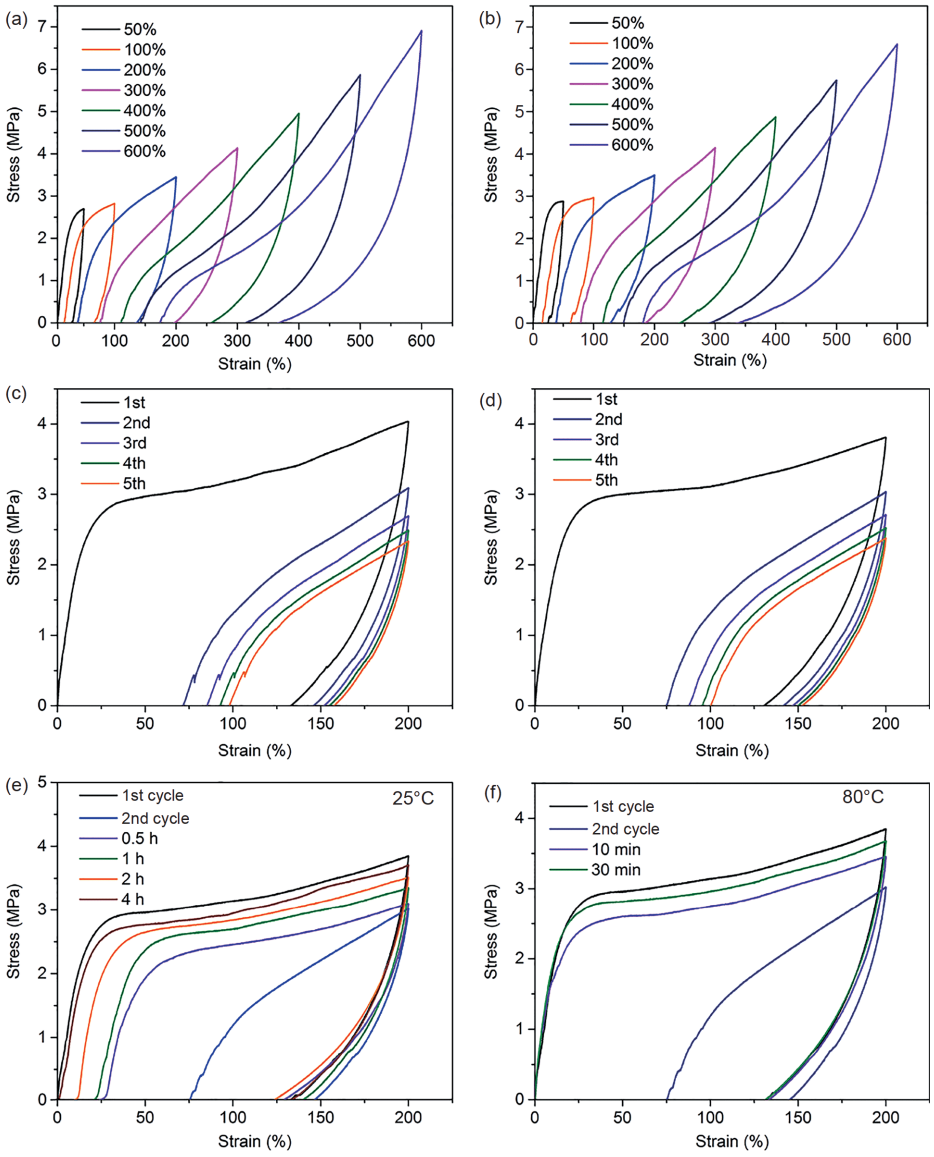

Figure 3 (Color online) (a) 7-times successive loading-unloading cycles of PDMS-PDITC$_{0.2}$-IPDI$_{0.8}$ and (b) the retested cycles after resting for 24 h at room temperature; (c) 5-times successive loading-unloading cycles of PDMS-PDITC$_{0.2}$-IPDI$_{0.8}$ and (d) the retested cycles after resting for 12 h at room temperature. The self-recovery of the loading-unloading curves of PDMS-PDITC$_{0.2}$-IPDI$_{0.8}$ for different resting times at (e) 25°C and (f) 80°C, respectively.

more operable in practical applications. Taking advantage of the unique features of PDMS-PDITC-IPDI, we first use it as transparent, recyclable adhesive for glass (Figure S13). The PDMS-PDITC-IPDI materials were placed between two glass plates and pressed to produce a uniform film by heating. Subsequent cooling to room temperature enabled the reformation of the hydrogen bonding network of PDMS-PDITC-IPDI. The adhesion strength was evaluated. As seen in Figure 5(a), with the increase of PDITC ratio, the adhesion strength increases first and then decreases. PDMS-PDITC$_{0.3}$-IPDI$_{0.7}$ showed the highest adhesion strength of 7.1 MPa. The possible reason is that when the ratio of PDITC is low, it is difficult to break more hydrogen bonds during the heating process due to its relatively low hard segment activity. With the increase of PDITC ratio, it is more likely to break hydrogen bonds during heating, thus obtaining higher adhesion strength. For PDMS-PDITC$_{0.4}$-IPDI$_{0.6}$, the low adhesion strength may attribute to relatively low mechanical property. In summary, the PDMS-PDITC-IPDI materials exhibited outstanding adhesive property comparable to other reported adhesives [46].

Our materials are 3D-printable at room temperature. Instead of universal high temperature extrusion 3D printing technique, the PDMS-PDITC-IPDI material can be printed through direct ink writing (DIW) 3D printing method, avoiding the possible impact of high temperature on material properties. Firstly, the PDMS-PDITC-IPDI material was dissolved in THF to prepare a high concentration solution.

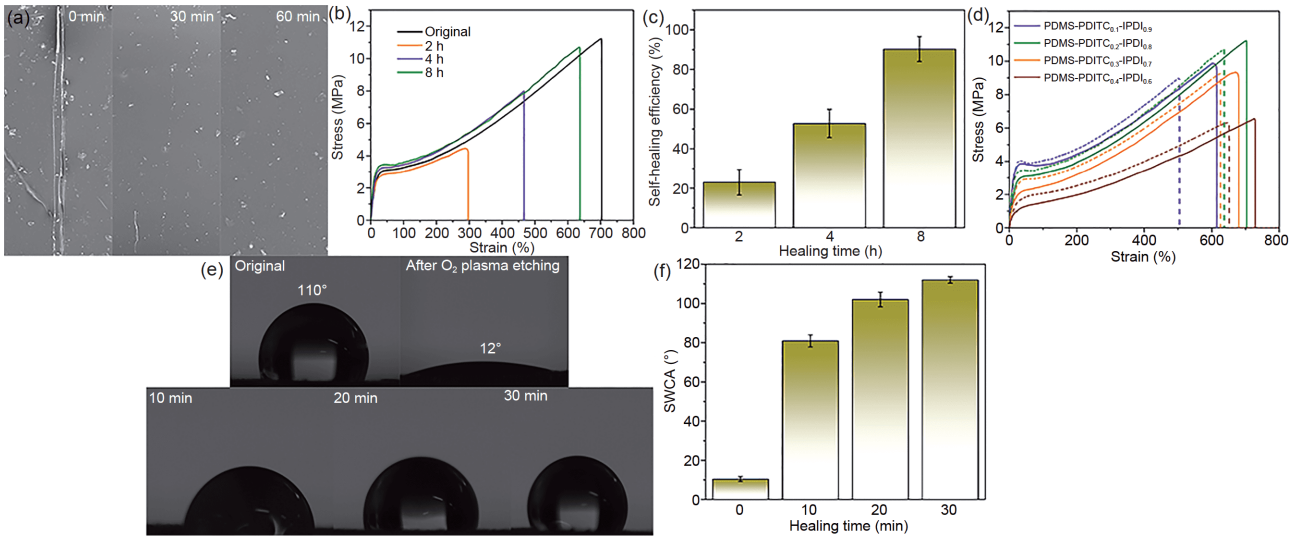

Figure 4 (Color online) (a) SEM images of the scratch of PDMS-PDITC$_{0.2}$-IPDI$_{0.8}$ at different self-healing times; (b) stress-strain curves and (c) the self-healing efficiencies of PDMS-PDITC$_{0.2}$-IPDI$_{0.8}$ at different self-healing times; (d) stress-strain curves of original and healed PDMS-PDITC-IPDI materials with different chemical composition; (e) SWCA and (f) the corresponding values of the original and plasma-etched PDMS-PDITC$_{0.2}$-IPDI$_{0.8}$ at different healing time at 100°C.

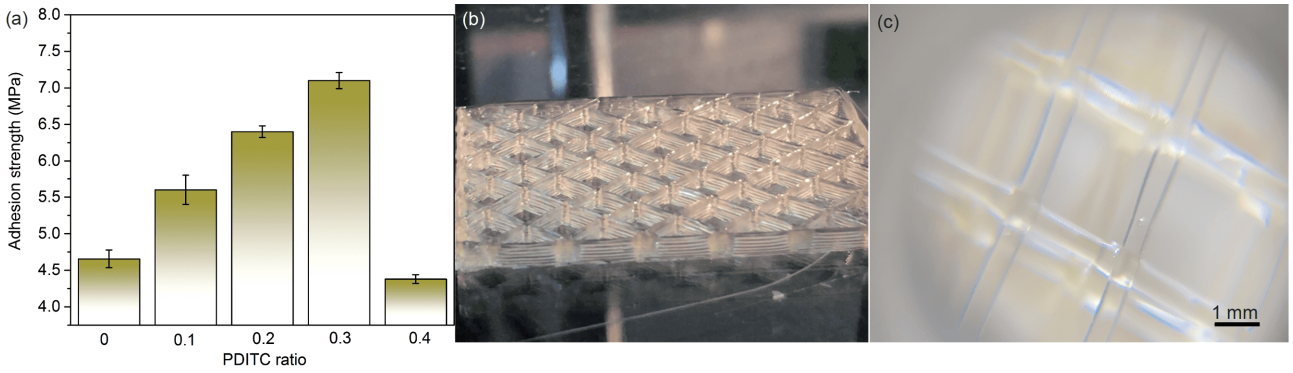

Figure 5 (Color online) (a) Comparison of adhesive strength between PDMS-PDITC-IPDI materials and PDMS-IPDI; (b) 3D-printed PDMS-PDITC-IPDI square grid; (c) the microphotograph of the 3D-printed PDMS-PDITC-IPDI square grid.

Then the solution was poured into a syringe mounted on a 3D printer. During the printing process, THF rapidly volatilized to ensure the dimensional stability. As shown in Figure 5(b), an 8 layers PDMS-PDITC-IPDI square grid was printed. Interlaced lines could be seen from the digital photograph for the 3D-printed material, showing the good 3D printing dimensional stability (Figure 5(c)). A video was provided in movie S1 to show the printing process. The facile 3D printing processability endows our material with broad application potential.

4 Conclusion

In summary, a novel dual-activate hard segment strategy is proposed for the fabrication of robust, tough, recyclable, chemical and mechanical healable polydimethylsiloxane based supramolecular material with 3D printing processability. The as-prepared PDMS-PDITC-IPDI materials exhibit tunable high toughness (43.1–24.5 MJ/m^3), tensile strength (11.3–6.6 MPa) and elongation at break (730%–615%) and possess excellent self-recovery capacity. Moreover, the PDMS-PDITC-IPDI materials show good mechanical self-healabiliy and hydrophobic recovery after chemical damage. The mechanical healing efficiency based on toughness reach above 90% within 8 h at 100°C. A scratch on the material surface can be completely healed within 30 min. After chemical damaged, the wettability of the material can restore to the original hydrophobic state within 30 min. As an exploration of the application, the materials are used as transparent, recyclable glass adhesive. The adhesion strength is up to 7.1 MPa. And the materials are 3D-printable at room temperature via a facile DIW 3D printing method. All the aforementioned properties make the

PDMS-PDITC-IPDI materials have great potential as a green functional material for sustainable development.

This work was supported by the National Natural Science Foundation of China (Grant No. 51473114), and the Natural Science Foundation of Tianjin (Grant No. 19JYCBJC17400).

Supporting Information

The supporting information is available online at tech.scichina.com and link.springer.com. The supporting materials are published as submitted, without typesetting or editing. The responsibility for scientific accuracy and content remains entirely with the authors.

1 Li Y, Ren M, Lv P, et al. A robust and flexible bulk superhydrophobic material from silicone rubber/silica gel prepared by thiol-ene photopolymerization. J Mater Chem A, 2019, 7: 7242–7255
2 Eduok U, Faye O, Szpunar J. Recent developments and applications of protective silicone coatings: A review of PDMS functional materials. Prog Org Coatings, 2017, 111: 124–163
3 Zhao J, Xu R, Luo G, et al. Self-healing poly(siloxane-urethane) elastomers with remoldability, shape memory and biocompatibility. Polym Chem, 2016, 7: 7278–7286
4 Lv C, Zhao K, Zheng J. A Highly stretchable self-healing poly(dimethylsiloxane) elastomer with reprocessability and degradability. Macromol Rapid Commun, 2018, 39: 1700686
5 Wang D P, Zhao Z H, Li C H, et al. An ultrafast self-healing polydimethylsiloxane elastomer with persistent sealing performance. Mater Chem Front, 2019, 3: 1411–1421
6 Liu C, Xie Q, Ma C, et al. Fouling release property of polydimethylsiloxane-based polyurea with improved adhesion to substrate. Ind Eng Chem Res, 2016, 55: 6671–6676
7 Lv C, Wang J, Li Z, et al. Degradable, reprocessable, self-healing PDMS/CNTs nanocomposite elastomers with high stretchability and toughness based on novel dual-dynamic covalent sacrificial system. Compos Part B-Eng, 2019, 177: 107270
8 Yan Q, Zhao L, Cheng Q, et al. Self-healing polysiloxane elastomer based on integration of covalent and reversible networks. Ind Eng Chem Res, 2019, 58: 21504–21512
9 Kang J, Son D, Wang G J N, et al. Tough and water-insensitive self-healing elastomer for robust electronic skin. Adv Mater, 2018, 30: 1706846
10 Liu L, Liang S, Huang Y, et al. A stretchable polysiloxane elastomer with self-healing capacity at room temperature and solvatochromic properties. Chem Commun, 2017, 53: 12088–12091
11 Jia X Y, Mei J F, Lai J C, et al. A highly stretchable polymer that can be thermally healed at mild temperature. Macromol Rapid Commun, 2016, 37: 952–956
12 Hoogenboom R. Hard autonomous self-healing supramolecular materials-a contradiction in terms? Angew Chem Int Ed, 2012, 51: 11942–11944
13 Li J, Zhang G, Deng L, et al. *In situ* polymerization of mechanically reinforced, thermally healable graphene oxide/polyurethane composites based on Diel-Alder chemistry. J Mater Chem A, 2014, 2: 20642–20649
14 Chen Q, Yan X, Zhu L, et al. Improvement of mechanical strength and fatigue resistance of double network hydrogels by ionic coordination interactions. Chem Mater, 2016, 28: 5710–5720
15 Yasui T, Kamio E, Matsuyama H. Inorganic/organic double-network ion gels with partially developed silica-particle network. Langmuir, 2018, 34: 10622–10633
16 Li X, Wang H, Li D, et al. Dual ionically cross-linked double-network hydrogels with high strength, toughness, swelling resistance, and improved 3D printing processability. ACS Appl Mater Interfaces, 2018, 10: 31198–31207
17 Wang Y J, Zhang X N, Song Y, et al. Ultrastiff and tough supramolecular hydrogels with a dense and robust hydrogen bond network. Chem Mater, 2019, 31: 1430–1440
18 Hu J, Mo R, Jiang X, et al. Towards mechanical robust yet self-healing polyurethane elastomers via combination of dynamic main chain and dangling quadruple hydrogen bonds. Polymer, 2019, 183: 121912
19 Li T, Zheng T Z, Guo Z X, et al. A well-defined hierarchical hydrogen bonding strategy to polyureas with simultaneously improved strength and toughness. Chin J Polym Sci, 2019, 37: 1257–1266
20 Wang H B, Li H F, Wu Y H, et al. A high strength, anti-fouling, self-healable, and thermoplastic supramolecular polymer hydrogel with low fibrotic response. Sci China Tech Sci, 2019, 62: 569–577
21 Wang D, Xu J H, Chen J Y, et al. Transparent, mechanically strong, extremely tough, self-recoverable, healable supramolecular elastomers facilely fabricated via dynamic hard domains design for multifunctional applications. Adv Funct Mater, 2020, 30: 1907109
22 Appel W P J, Portale G, Wisse E, et al. Aggregation of ureido-pyrimidinone supramolecular thermoplastic elastomers into nanofibers: A kinetic analysis. Macromolecules, 2011, 44: 6776–6784
23 Xu J H, Chen P, Wu J W, et al. Notch-insensitive, ultrastretchable, efficient self-healing supramolecular polymers constructed from multiphase active hydrogen bonds for electronic applications. Chem Mater, 2019, 31: 7951–7961
24 Wu X, Wang J, Huang J, et al. Robust, stretchable, and self-healable supramolecular elastomers synergistically cross-linked by hydrogen bonds and coordination bonds. ACS Appl Mater Interfaces, 2019, 11: 7387–7396
25 Zhang Y, Yuan L, Liang G, et al. Simultaneously achieving superior foldability, mechanical strength and toughness for transparent healable polysiloxane films through building hierarchical crosslinked networks and dual dynamic bonds. J Mater Chem A, 2018, 6: 23425–23434
26 Liu X, Wang K, Zhang W, et al. Robust, self-cleaning, anti-fouling, superamphiphobic soy protein isolate composite films using spray-coating technique with fluorinated HNTs/SiO_2. Compos Part B-Eng, 2019, 174: 107002
27 Cao N, Guo J Y, Boukherroub R, et al. Robust superhydrophobic polyurethane sponge functionalized with perfluorinated graphene oxide for efficient immiscible oil/water mixture, stable emulsion separation and crude oil dehydration. Sci China Tech Sci, 2019, 62: 1585–1595
28 Fu Y, Xu F, Weng D, et al. Superhydrophobic foams with chemical- and mechanical-damage-healing abilities enabled by self-healing polymers. ACS Appl Mater Interfaces, 2019, 11: 37285–37294
29 Qin L, Chen N, Zhou X, et al. A superhydrophobic aerogel with robust self-healability. J Mater Chem A, 2018, 6: 4424–4431
30 Yanagisawa Y, Nan Y, Okuro K, et al. Mechanically robust, readily repairable polymers via tailored noncovalent cross-linking. Science, 2018, 359: 72–76
31 Zhao J, Xu R, Luo G, et al. A self-healing, re-moldable and biocompatible crosslinked polysiloxane elastomer. J Mater Chem B, 2018, 4: 982–989
32 Cui J, Daniel D, Grinthal A, et al. Dynamic polymer systems with self-regulated secretion for the control of surface properties and material healing. Nat Mater, 2015, 14: 790–795
33 Jia X Y, Mei J F, Lai J C, et al. A self-healing PDMS polymer with solvatochromic properties. Chem Commun, 2015, 51: 8928–8930
34 Zhang A, Yang L, Lin Y, et al. Self-healing supramolecular elastomers based on the multi-hydrogen bonding of low-molecular polydimethylsiloxanes: synthesis and characterization. J Appl Polym Sci, 2013, 129: 2435–2442
35 You Y, Huang W, Zhang A, et al. A facile and controllable synthesis of dual-crosslinked elastomers based on linear bifunctional polydimethylsiloxane oligomers. J Polym Sci Part A-Polym Chem, 2016, 54: 3760–3768
36 Rao Y L, Chortos A, Pfattner R, et al. Stretchable self-healing polymeric dielectrics cross-linked through metal-ligand coordination. J Am Chem Soc, 2016, 138: 6020–6027

37 Wang D P, Lai J C, Lai H Y, et al. Distinct mechanical and self-healing properties in two polydimethylsiloxane coordination polymers with fine-tuned bond strength. Inorg Chem, 2018, 57: 3232–3242
38 Lai J C, Mei J F, Jia X Y, et al. A stiff and healable polymer based on dynamic-covalent boroxine bonds. Adv Mater, 2016, 28: 8277–8282
39 Li C H, Wang C, Keplinger C, et al. A highly stretchable autonomous self-healing elastomer. Nat Chem, 2016, 8: 618–624
40 Zhang D D, Ruan Y B, Zhang B Q, et al. A self-healing PDMS elastomer based on acylhydrazone groups and the role of hydrogen bonds. Polymer, 2017, 120: 189–196
41 Liu M, Liu P, Lu G, et al. Multiphase-assembly of siloxane oligomers with improved mechanical strength and water-enhanced healing. Angew Chem Int Ed, 2018, 57: 11242–11246
42 Wu T, Chen B. Synthesis of multiwalled carbon nanotube-reinforced polyborosiloxane nanocomposites with mechanically adaptive and self-healing capabilities for flexible conductors. ACS Appl Mater Interfaces, 2016, 8: 24071–24078
43 Lai J C, Li L, Wang D P, et al. A rigid and healable polymer cross-linked by weak but abundant Zn(II)-carboxylate interactions. Nat Commun, 2018, 9: 2725
44 Cao P F, Li B, Hong T, et al. Superstretchable, self-healing polymeric elastomers with tunable properties. Adv Funct Mater, 2018, 28: 1800741
45 Liu J, Wang S, Tang Z, et al. Bioinspired engineering of two different types of sacrificial bonds into chemically cross-linked *cis*-1,4-polyisoprene toward a high-performance elastomer. Macromolecules, 2016, 49: 8593–8604
46 Liu M, Wang Z, Liu P, et al. Supramolecular silicone coating capable of strong substrate bonding, readily damage healing, and easy oil sliding. Sci Adv, 2019, 5: eaaw5643